Methodology Development for BEV HV-Battery Durability Analysis based on Vehicle Dynamics

Luís Miguel Ferreira Figueiredo
luis.figueiredo.98@tecnico.ulisboa.pt

Instituto Superior Técnico, Universidade de Lisboa, Portugal

November 2021

Abstract

The main focus of this work is to propose a new procedure for structural simulation of HV (High-Voltage) batteries. Currently, OEMs (Original Equipment Manufacturers) resort to shaker machines to carry out vibration tests on HV batteries. These sorts of tests were widely used for small batteries. However, the recent increase of the degree of electrification and the demand for longer-lasting batteries has lead to an increase of their size and weight. In fact, these batteries can now weight more than 600 Kg and have a 2 m length, therefore interfering with the overall dynamics of the car [2]. It is believed that, resorting to shaker machines to test these batteries leads to an under-estimation of the damage generated in the battery, because in reality, the battery undergoes global deformations, as it bends and twists together with the bodywork.

This work aims to compare the accelerations measured in certain points of the battery for 3 different cases: a shaker test simulation, an experimental shaker test and full-vehicle simulations with an integrated battery model. The latter aims to approximate the behaviour of the battery in a life-representative situation. The pseudo-damage will then be calculated for each situation. It was found that the vehicle-level simulation can be up to 80 times more damaging than a battery-level shaker test.

Keywords: HV-Battery, Durability, Dynamic Simulation, Full-Vehicle Model, Pseudo-damage

1. Introduction

Electric and hybrid vehicles have been pointed by the European Union as important tools to decrease the emissions of greenhouse gases. Fleet-wide CO_2 emission restrictions and gasoline and diesel-powered car bans are some of the measures currently applied to aid the decrease of greenhouse gas emissions. Due to these new regulations and customer demand as well, the automotive industry is undergoing a shift towards the implementation of electric powertrains in automobiles [4].

Additionally, automotive manufacturers are obligated to design vehicles that can operate safely under regular and predicted events that take place during the working life of the vehicle [2]. Especially, novel components like the HV battery require special attention. These batteries have become very large and heavy, given the increase of both the degree of electrification of the automobiles and the expected charge duration of the battery. For this reason, they can no longer be tested using the current existing procedures destined to test smaller batteries.

Despite of the new sizing and weight of these batteries, OEM's still resort to previously known procedures in the industry to submit the HV batteries to structural testing. One of the most common procedures is the shaker test, in which the battery is stiffly connected to a table and unidirectionally shaked with a gaussian acceleration time signal. This testing procedure is believed to be inappropriate for large HV-Batteries, because, in reality, the battery is connected to a flexible chassis that deforms due to road dynamic excitations. Therefore, the battery deforms globally, instead of being simply shaked. Furthermore, Rissoan [5] has concluded that most of the real-life acceleration measurements performed in life-representative conditions of automobiles revealed non-gaussian characteristics, bringing and additional unforeseeable damage contribution to chassis-mounted components like the HV battery.

This work presents a suggestion of a new simulation procedure to account for damage contribution generated by the global deformations on the battery. The new procedure consists of a vehicle-level simulation with a flexible chassis including a model of the HV-Battery. In the simulation, the vehicle model travels across 5 different types of

roads, in order to create a life-representative loading of the battery. 3 different scenarios are compared in this project: a battery shaker test, in which the battery is shaken vertically as an acceleration gaussian time signal is imposed to it; a shaker test simulation, acting as a digital twin of the actual test; and full-vehicle simulations, in which the battery finite element model is integrated in the chassis and the full-vehicle assembly is simulated in different road types. To observe the general deformations of the battery, the most contributing mode shapes and respective modal participation factors for each dynamic simulation will be compared. Apart from that, a comparison of the acceleration time-signals in different points of the battery will be carried. From these time signals, a pseudo-damage parameter will be calculated so that a comparative analysis of the load severity is achieved.

The objectives for this thesis can hereby be defined:

- To develop a simplified beams model with similar modal properties as the detailed BiW model.
- To determine and compare the mode shapes that dominate the dynamic analyses and modal participation.
- To measure and compare the accelerations obtained from the dynamic simulations and shaker test.
- To calculate and compare the pseudo-damage generated from the full-vehicle simulations with the one from the battery shaker test.

Figure 1 presents the general workflow followed during this project.

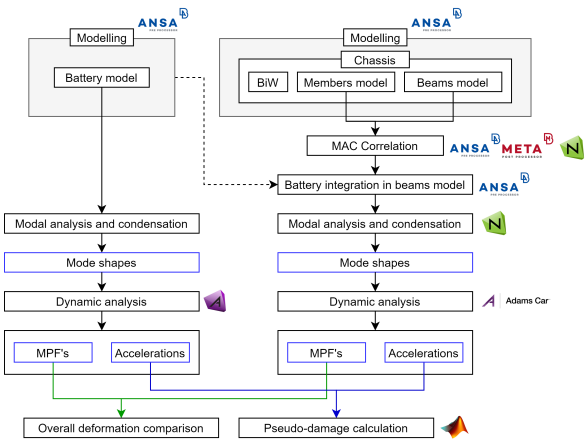

Figure 1: Schematic thesis workflow

2. Backgorund

2.1. Dynamic analysis

The governing equations for a dynamic analysis are shown in the matricial form in equation 1.

$$[M]\{\ddot{u}\} + [C]\{\dot{u}\} + [K]\{u\} = \{f\}(t) \tag{1}$$

2.2. Modal Analysis

A modal analysis is a particular type of dynamic analysis, in which the damping influence is neglected and the external forces are null. The governing equation for the modal analysis is given in equation 2. The solution of this equation is a sinusoidal signal given by equation 3. The replacement of the $\{u\}$ vector in equation 2 results in the eigenvalue problem given by equation 4. The eigenvalues obtained from this equation correspond to the square of the angular frequencies and the eigenvectors are the correspondent mode shapes.

$$[M]\{\ddot{u}\} + [K]\{u\} = \{0\} \tag{2}$$

$$\{u\} = \{\phi\}sin(\omega t) \tag{3}$$

$$([M]\omega^2 - [K])\{\phi\} = \{0\} \tag{4}$$

2.3. Guyan reduction

The Guyan reduction method is generally used to reduce the computational effort of a dynamic analysis. This method consists of a re-organization of the governing equation (equation 1) so that the number of computed DOFs (Degrees of Freedom) is smaller, leading to smaller computation times. The governing equation is re-written according to equation 5. By re-organizing the second line of equation 5 and replacing it on the first line, equation 6 is obtained. The latter only requires calculations involving the master (m) nodes of the finite element component.

$$\begin{bmatrix} [K_{mm}][K_{ms}] \\ [K_{sm}][K_{ss}] \end{bmatrix} \begin{Bmatrix} u_m \\ u_s \end{Bmatrix} = \begin{Bmatrix} f_m \\ \{0\} \end{Bmatrix} \tag{5}$$

$$([K_{mm}] - [K_{ms}][K_{ss}]^{-1}[K_{sm}])\{u_m\} = \{f\} \tag{6}$$

2.4. Modal superposition

The modal superposition method suggests that the deformation of a body during a dynamic analysis can be given as a linear combination of the eigenmodes of that body, as follows:

$$\{u\} = \sum_i y_i \phi_i \tag{7}$$

Where ϕ_i is the mode shape of mode i and y_i is the respective MPF (Modal Participation Factor).

2.5. Modal Assurance Criterion

The Modal Assurance Criterion (MAC) is used to correlate the mode shapes of two similar structures by associating the displacements (DOF's 1,2 and 3) of two comparable sets of nodes in the structure. The MAC value should always be a number between 0 and 1. The closer this value is to 1, the better the correlation is, i.e. the more similar the mode shapes are. The MAC is calculated according to equation 8. r and q denote the numbers of the modes in models A and X, respectively.

$$MAC = \frac{|\{\phi_A\}_r^T \{\phi_A\}_q|^2}{(\{\phi_A\}_r^T \{\phi_A\}_r)(\{\phi_X\}_q^T \{\phi_X\}_q)} \tag{8}$$

2.6. Shaker test

In this test, the battery is bolted to a stiff table which vibrates unidirectionally due to a gaussian white noise excitation (random vibration). Figure 2 presents the configuration for the shaker test.

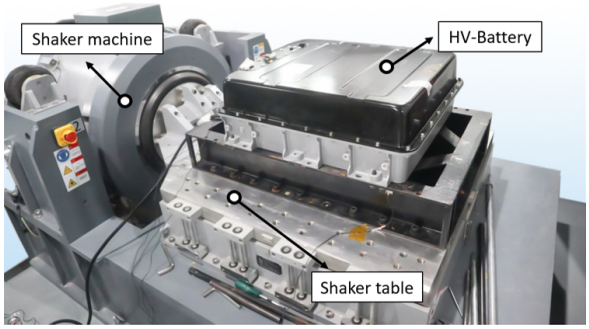

Figure 2: Shaker test configuration

2.7. PSD profile

A PSD (Power Spectral Density) consists of a normalization of the fast fourier transform of a random time signal with respect to the frequency sampling rate, so that the dependency of the time signal duration is lost. That way, PSD's derived from signals that have different time lengths can be compared.

2.7.1 Standards of PSD profiles for HV-Battery vibration testing

In this project, only the ISO 12405-1 standard will be analysed, since it is one of the most common standards in the automotive industry for HV-Battery vibration testing, highly requested by OEM's. Figure 3 presents the PSD profile established by the ISO 12405-1 standard. Only the PSD defined for the z-direction was considered in this project.

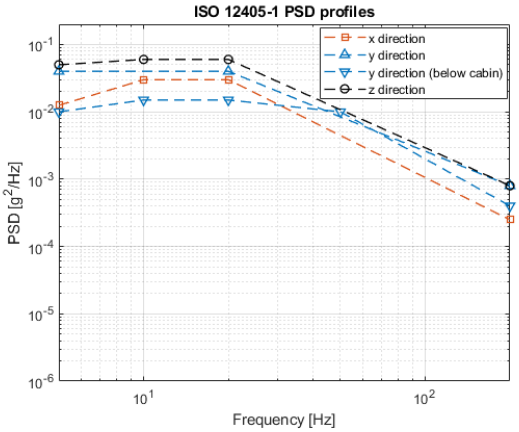

Figure 3: ISO 12405-1 PSD profiles

2.8. Gaussian time signals

Standardized PSD procedures require that the frequency-to-time-domain conversion of the excitation load originates a gaussian signal. These signals can be fully characterised by their mean value (μ) and the variance (σ^2).

2.9. Non-gaussian parameters

2.9.1 Kurtosis coefficient (γ_2)

This parameter measures the flatness of the PDF (Probability Density Function) around its mean value and it is given by equation 9. Gaussian signals have a null kurtosis coefficient. If γ_2 is positive, the time signal is known as leptokurtic. Acceleration measurements that are leptokurtic usually generate more damage than gaussian ones despite of having the same PSD [5].

$$\gamma_2 = \frac{E[X-\mu]^4}{\sigma^4} - 3 \tag{9}$$

2.10. Crest Factor

This parameter is given by the maximum absolute value of a sample divided by the RMS (Root-Mean Square) value of that sample, as defined in equation 10.

$$CF = \frac{X_{peak}}{X_{RMS}} = \frac{\max(|X|)}{\sqrt{\{X\}^2}} \tag{10}$$

2.11. Pseudo-Damage

White noise time signals consist of a combination of load cyles. These load cycles are obtained by the rainflow counting method and have specific mean and peak values that are used by pseudo-damage concept to evaluate the load severity. The pseudo-damage expression is derived from the Basquin's rule for a S-N curve [1] and it is given by equation 11, where S_i corresponds to the amplitude of cycle i. β is set to 5 as a thumb-rule defined in [1].

$$d = \sum_i S_i^\beta \tag{11}$$

3. HV-Battery model

The vehicle model considered in this thesis is the Audi E-tron 55 Quattro Edition One 2019. It is a BEV (Battery Electric Vehicle), with a 681.26 Kg battery placed under the cabin (see figure 4). This battery stores 95 KWh of energy and has a nominal voltage of 396 V. The battery and its main dimensions can be seen in figure 5. For the development of the finite element model of the battery, only the most relevant components from the structural point of view were considered. The finite element model can be seen in figure 6

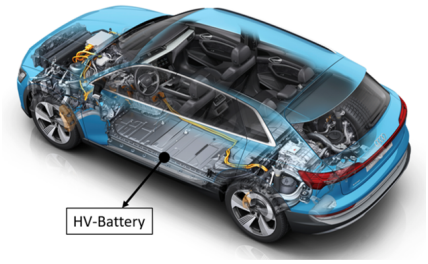

Figure 4: Battery location in the Audi E-tron model (courtesy of autoprova.be)

3.1. Mass Comparison

Table 1 shows that the mass difference between the finite element model and the actual battery is 1.84 Kg (0.27%), which is considered as acceptable for this purpose.

Table 1: Mass comparison between the actual battery and the finite element model

	HV-Battery	Finite element model
Mass [Kg]	681.26	679.42

3.2. Mode shape comparison

With resort to a hammer test, the first bending and torsion mode shapes were captured as well as the respective frequencies. In this section, these results are compared with the ones obtained in the modal analysis in Nastran. The mode shape comparison can be seen in figure 7. It is possible to see that the global deformation of the battery appears to be correctly captured. Local deformations were not detected in the hammer test. Table 2 presents a comparison of the measured vibration frequencies with the ones obtained from the modal analysis. The maximum relative error is 9.32%, which is considered to be acceptable given the simplifications done in the battery finite element model.

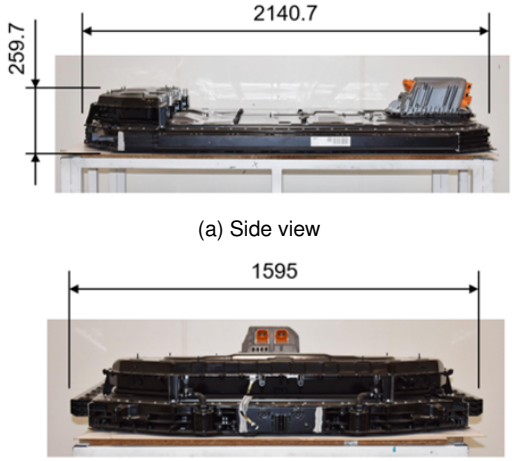

(a) Side view

(b) Rear view

Figure 5: HV-Battery (courtesy of A2Mac1)

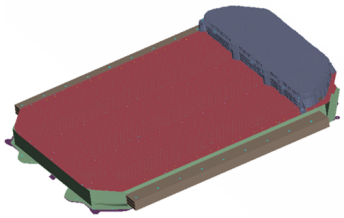

Figure 6: Finite element model of the battery

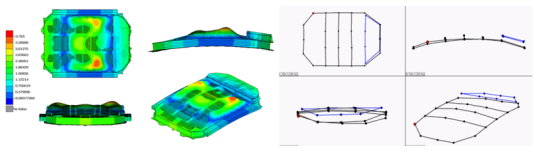

(a) 1st bending mode: Modal analysis (left) and hammer test (right)

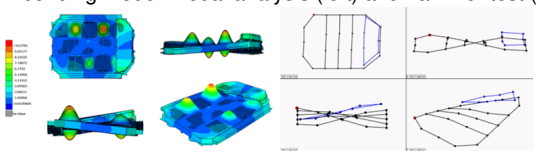

(b) 1st torsion mode: Modal analysis (left) and hammer test (right)

Figure 7: Mode shape comparison

Table 2: Natural frequency comparison for the first bending and torsion mode of the battery

	1st Bending	1st Torsion
Simulated frequency [Hz]	45.34	61.76
Measured frequency [Hz]	50	60
Absolute error [Hz]	4.66	5.95
Relative error [%]	9.32	2.93

3.3. Chassis models

From the BiW (Body in White) model, a simplified model constituted by beam elements is intended to be created. The beams model must have a similar dynamic behaviour as the BiW but with a much lower computational effort involved. The workflow to create the beams model is presented in figure 8. The conversion from 2D and 3D to 1D elements was done using the *Epilysis* tool available in ANSA pre-processor. Table 3 provides a comparison in terms of mass between the aforementioned models. The beams model mass is lower than the BiW (15.96% lower), however, in section 3.3.2, the concentrated masses will be added to the beams model to account for components disregarded in the simplification process.

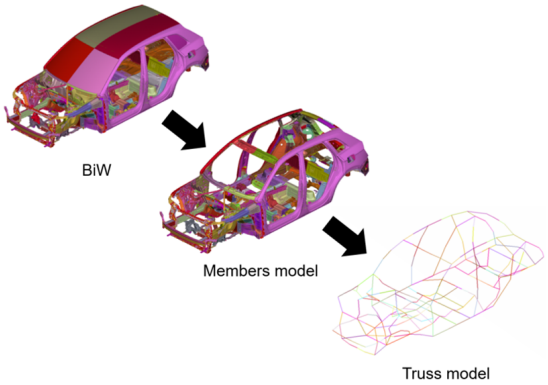

Figure 8: BiW to beams model conversion

Table 3: Mass comparison between the BiW, Members and beams model

	BiW	Members Model	Beams Model
Mass [Kg]	526.12	396.93	442.13

3.3.1 MAC validation of the beams model

The MAC correlation tool availabe in META post-processor was used to compare the mode shapes and frequencies from the members model and the beams model. For all modal analyses, modes 1 to 6 were neglected due to the fact that they are rigid-body modes. The MAC correlation nodes were selected at key locations shown in figure 9. The results obtained from this correlation are shown in figure 10. In this figure, the secondary matrix diagonal is of particular interest, since the highest MAC and lowest frequency difference results are intended to be seen there. The results show a good correspondence of the mode shapes for modes 7, 8 and 9 (MAC $>$ 80%). The remaining modes have lower MAC's, which is believed to be a consequence of not considering the side-panels of the car in the members model, affecting both the mass and stiffness of this model. This factor also affects the results in the frequency difference matrix, it is possible that modes 7, 8, 10 and 12 vibrate at frequencies that have a 32 to 44% difference. Modes 9 and 11 show a smaller relative frequency difference.

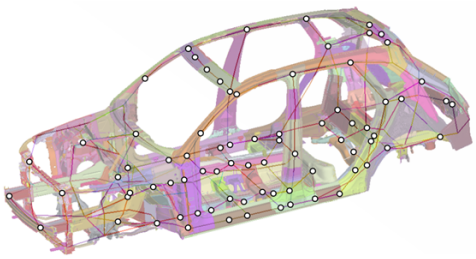

Figure 9: MAC correlation nodes

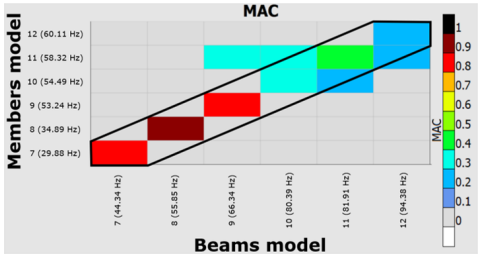

(a) MAC values

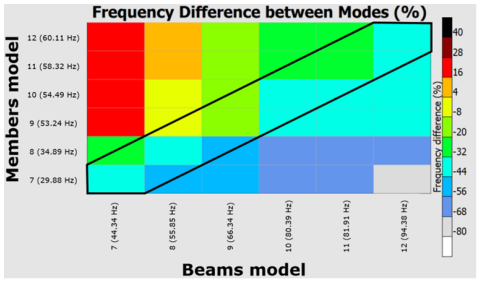

(b) Relative frequency difference

Figure 10: MAC correlation results

3.3.2 Battery integration in the beams model

The integration of the battery was done with resort to rigid elements. 35 connections were done. The connections were organized in 5 different groups based on their location, as shown in figure 11.

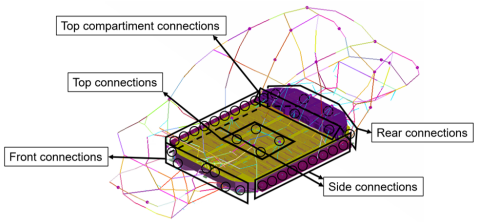

Figure 11: Battery-to-beams-model connections

3.3.3 Concentrated masses in the beams model

Due to the simplifications done to obtain the beams model, it is now necessary to add the masses that were neglected before so that the mass of the unloaded beams-battery and unloaded BiW-battery models match. The unlodaded models do not account with the passengers' weight. Figure 12 displays the locations in which the masses were added as well as the value of each mass. Table 4 shows that the mass difference of the considered models is 95.29 Kg (7.89%).

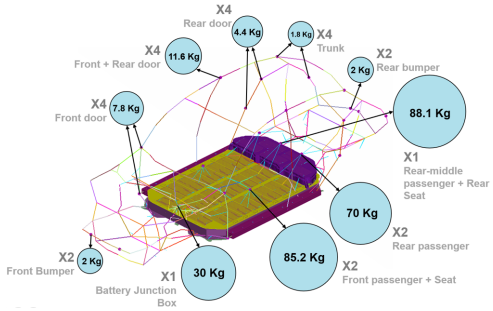

Figure 12: Concentrated mass locations and values

Table 4: Mass comparison between the unloaded Beams-Battery and BiW-Battery models

	BiW-Battery	Beams-Battery
Mass [Kg]	1208.19	1303.48

3.4. Full-vehicle model

The suspension model is the starting point for the full-vehicle model generation. All the remaining components were imported to the suspension model in order to create the full-vehicle assembly. The only flexible components considered in the suspension are the ARB's (anti-roll-bars). The full-vehicle assembly can be seen in figure 13.

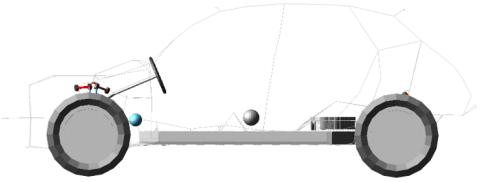

Figure 13: Full-vehicle model

4. Analysis configuration

4.1. Battery shaker simulation

The battery is connected to the shaker table by 26 sherical joints. A vertical point motion is applied to the shaker table in its center of mass. This point motion applies the white noise extracted from the ISO 12405-1 PSD profile sampled in 8001 points during 10 seconds. 14 modes were considered for the modal superposition (modes 7 to 20).

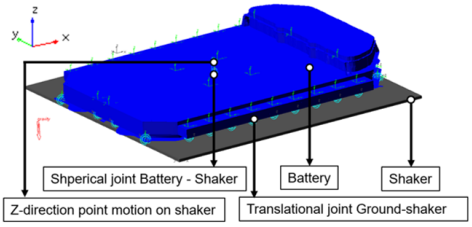

Figure 14: Battery shaker simulation setup

4.2. Full-vehicle simulation

The setup for the full-vehicle simulations involves imposing a constant velocity to the vehicle while it travels across 5 different road types. Only 27 modes were considered (modes 7 to 34 without mode 8). Mode 8 was excluded for representing a local deformation in a beam member, without any deformation in the battery. The setup for the full-vehicle simulations is shown in figure 15. The simulation characteristics for each road type are specified in table 5. The time step for all full-vehicle simulations is set to be 0.025 s.

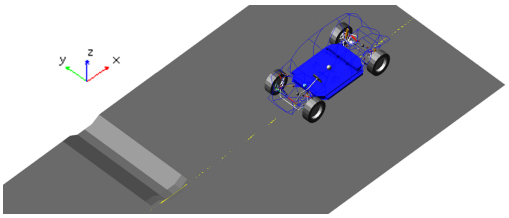

Figure 15: Full-vehicle simulation setup

Table 5: Full-vehicle simulation characteristics

Road profile	Vehicle velocity $[Km/h]$	Simulation time $t_{sim}[s]$	Distance covered $d_{sim}[m]$
Pothole	30	10	83.3
D-class road	60	10	166.7
Washboard In-Phase	40	10	111.1
Washboard Out-of-Phase	40	10	111.1
Cobblestone road	40	10	111.1

5. Results

5.1. Modal Participation Factors

Figure 16 shows the RMS (Root-Mean Square) values for the MPF's for all the modes that were considered in the battery and full-vehicle simulations. The battery MPF values appear to be 9 orders of magnitude smaller the ones from the vehicle simulation. This is due to the high level of constraint of the shaker simulations, preventing large motions and, therefore, large modal participation. In the full-vehicle simulations, the pothole, D-class road and cobblestone generate the highest overall mode participation. The most participating mode for these cases is mode 9. This mode shape is shown in figure 17, from which it is possible to see it is a torsion mode that globally deforms the battery.

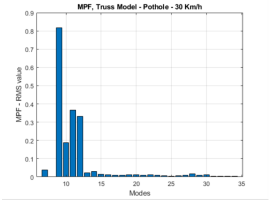

(a) Full vehicle simulation - Pothole

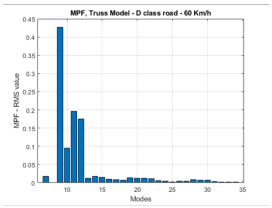

(b) Full vehicle simulation - D-class road

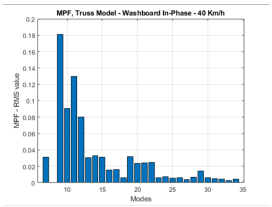

(c) Full vehicle simulation - Washboard In-Phase

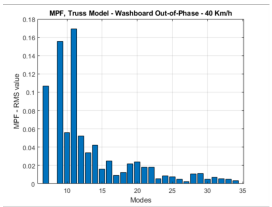

(d) Full vehicle simulation - Washboard Out-of-Phase

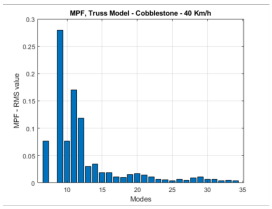

(e) Full vehicle simulation - Cobblestone

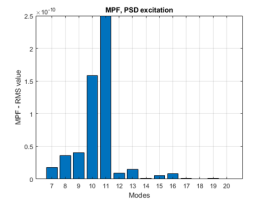

(f) Battery shaker simulation

Figure 16: RMS MPF values obtained from the full-vehicle and battery shaker simulations

5.2. Acceleration measurements

The accelerations were obtained for all the full-vehicle simulations, battery simulation and battery shaker test. These accelerations were measured in 4 specific points. These points are identified by their ID's in figure 18. Hereinafter, these nodes will be referred to by their last 3 digits.

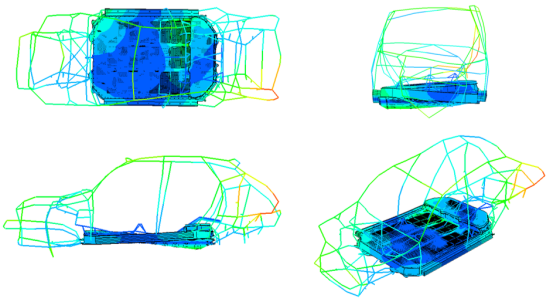

Figure 17: Mode 9 - Beams-battery model

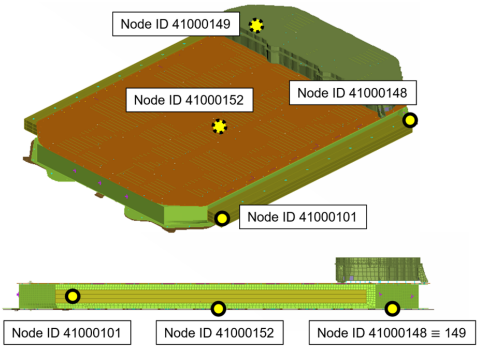

Figure 18: Location of the nodes for the acceleration measurement

5.3. Kurtosis coefficient comparison

The kurtosis coefficients were measured for each of the acceleration time signals and are compared in table 6. The kurtosis of the shaker simulation is the same for all nodes and equal to 1.05 due to the fact that all of these nodes are being imposed the same displacement, and therefore, have the same acceleration, and the same kurtosis coeficient. The shaker test produced acceleration measurements that have an almost-zero kurtosis coefficient (quasi-gaussian signals).

The road that appears to be generating the highest overall kurtosis coefficients, and, therefore, the most leptokurtic load is the pothole. Node 152 stands out for being the less prone to register a leptokurtic loading, which is a result of its central position in the battery, away from the suspension-provenient loadings.

Table 6: Comparison of the kurtosis coefficient for the different vertical acceleration measurements

		Node ID			
		101	**152**	**148**	**149**
Battery shaker simulation		1.05	1.05	1.05	1.05
Battery shaker test		-0.17	-0.12	-0.09	-0.15
Full-vehicle simulations	**Pothole**	12.95	9.04	17.28	17.28
	D-class Road	2.92	0.69	0.83	1.40
	Washboard I.P.	-0.34	0.68	-0.74	-1.14
	Washboard O.P.	31.10	-0.92	-0.61	0.28
	Cobblestone	2.03	1.93	4.65	0.75

5.4. PSD comparison

The PSD's from all vertical accelerations from the dynamic simulations and test are compared in figure 19 for all 4 considered nodes. In this figure, it is possible to see that the battery simulation PSD remains unchanged between all considered nodes, which is a result of measuring the accelerations at the connections between the shaker and the battery. All of these nodes have the same acceleration time signal and respective PSD. The PSD obtained experimentally from the shaker test cannot be explicitly revealed due to customer data protection. However, the blurred contour of this PSD (gray area in figure 19) shows that there is a good correlation between the simulated and experimental PSDs.

From the vehicle simulations, it is possible to see that there is an overall predominance from the cobblestone road. Furthermore, the PSD's that behave more erratically (washboard roads) are also the ones that excite the modes more evenly, i. e., they have the largest relative contribution from higher modes (see figure 16). All of the full-vehicle PSD's end at 20 Hz, which is a limitation associated to the time step of the vehicle simulations. According to the Nyquist-Shannon Sampling Theorem [6], this time step should be, at least, 10 times smaller ($t_{step(new)}$ = 0.0025 s).

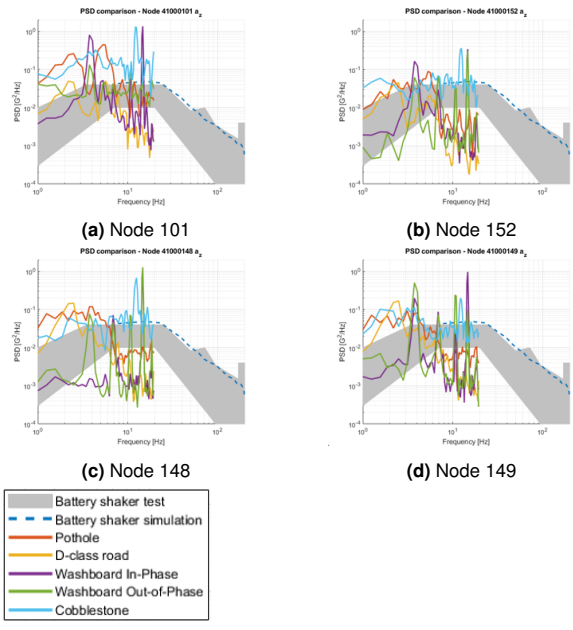

(a) Node 101 **(b)** Node 152 **(c)** Node 148 **(d)** Node 149 **(e)** Legend

Figure 19: RMS MPF values obtained from the full-vehicle and battery shaker simulations

5.5. Acceleration result normalization

The battery simulation, battery shaker test and full-vehicle simulations acceleration time signals correspond to different quantities of vehicle usage. In order to correctly compare the pseudo-damage obtained from these accelerations, the simulations and test must be normalized to be representative of the same vehicle usage distance. The value chosen for the normalization is 100 000 miles (160 934 Km).

This amount of vehicle usage corresponds to shaker testing the HV-Battery in accordance to standard SAE J2380 [3]. An assumption is made in this project that ISO 12405-1 produces a comparable amount of pseudo-damage as the SAE standard. This assumption is supported by the fact that SAE J2380 uses slightly higher PSD amplitudes and lower testing times than ISO 12405-1. The test duration according to ISO 12405-1 is 21h. Therefore, the time signal from the battery shaker simulation (originally lasting 10 s) is replicated 7560 times; and the time signal from the battery shaker test (originally lasting 60 s) is replicated 1260 times.

For the full-vehicle simulations, the different types of roads had to be averaged according to the procedure in [3]. The number of repetitions of each sort of road to make up 100 000 miles of vehicle testing are shown in table 7

Table 7: Calculation of the number of repetitions for each of the vehicle simulations

Road profile	Track length [m]	Final participation [Km]	Number of repetitions
Pothole	83.3	6958.8	83539
D-class road	166.7	6958.8	41744
Washboard In-Phase	111.1	27836.8	250556
Washboard Out-of-Phase	111.1	56109.6	505037
Cobblestone road	111.1	63068.4	567672
Total	583.3	161032.4	1448548

5.6. Pseudo-damage calculation

The rainflow counting method was applied to the normalized acceleration time signals so that a contabilization of the amount of cycles and their amplitude was determined. From the battery-level analyses, only the shaker test results will be considered for the pseudo-damage calculations since the PSD comparison predicts a much larger amount of damage in the shaker test than in the shaker simulation. From these cycles, the pseudo-damage concept was applied. A visualization of the pseudo-damage in logarithmic scale is shown in figure 20. From this figure, it is possible to see that the full-vehicle simulations generate a larger amount of accumulated pseudo-damage than the shaker test. A

detailed analysis of the pseudo-damage contribution of each road type for the total pseudo-damage is done in table 8. Table 9 presents the amount of times the vehicle simulation pseudo-damage is greater than the battery shaker test one. It is possible to conclude that the most damaging road is, generally, the cobblestone, which is also the road that has the largest amount of repetitions. The D-class road is the least damaging road for all considered nodes. Finally, it is possible to conclude that the full-vehicle simulations can be from 4 to 80 times more damaging than the battery shaker test when both the simulations and test are normalized to the same amount of vehicle usage.

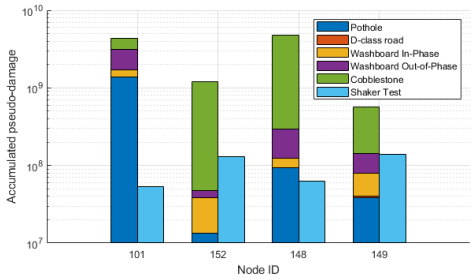

Figure 20: Accumulated pseudo-damage comparison between the full-vehicle simulations (left stack) and the battery shaker test (right stack)

Node ID		41000101	41000152	41000148	41000149
Battery shaker test measurements Pseudo-damage		5.39E+07	1.28E+08	6.35E+07	1.38E+08
Vehicle simulations Pseudo-damage	Pothole	1.37E+09	1.33E+07	9.32E+07	3.88E+07
	D-class road	2.70E+06	2.09E+05	1.27E+06	1.57E+06
	Washboard I.P.	3.46E+08	2.47E+07	3.03E+07	3.92E+07
	Washboard O.P.	1.44E+09	9.02E+06	1.72E+08	6.34E+07
	Cobblestone	1.16E+09	1.16E+09	4.45E+09	4.31E+08
	TOTAL (Vehicle simulations)	**4.32E+09**	**1.21E+09**	**4.75E+09**	**5.74E+08**

Table 8: Absolute Pseudo-damage contribution form each type of road

Node ID		41000101	41000152	41000148	41000149
Vehicle simulations Pseudo-damage	Pothole	25.42	0.10	1.47	0.28
	D-class road	0.05	1.63E-03	0.02	0.01
	Washboard I.P.	6.41	0.19	0.48	0.28
	Washboard O.P.	26.73	0.07	2.70	0.46
	Cobblestone	21.51	9.04	70.13	3.12
	TOTAL	**80.12**	**9.40**	**74.80**	**4.16**

Table 9: Relative Pseudo-damage contribution form each type of road

6. Conclusions

From the results presented in this work, it is possible to conclude that the vehicle-level simulations, that lead to global deformations in the battery pack are, indeed, more damaging than the shaker test that is carried at battery-level. The full-vehicle simulations have shown to be up to 80 times more damaging than the current HV-battery vibration testing procedures used in the automotive industry.

6.1. Future work

The beams model developed in the modelling stage of this work only shows a good MAC correlation for the mode shapes of the first 3 considered modes. Further development of this model is needed so that all mode shapes can be properly correlated. Furthermore, shell structures could be added to the beams model to account for the panels that were removed in the simplification process. This would possibilitate a correlation between the beams model and the BiW, therefore improving the trustworthiness of the beams model.

Only 5 road types were considered for the full-vehicle simulations carried in this project. A broader diversity of road types could have been used, in line with the road types available at proving ground test facilities.

HV-Battery vibration testing is a continuously developing topic. Therefore, the standards used by OEM's to test their batteries change often as they suffer adjustments to further improve the shaker test methodology. A more recent shaker test PSD profile standard could have been used so that a more up-to-date comparison of damage was achieved. Additionally, the shaker test could have also been simulated in accordance with SAE J2380 so that a 100000-mile-representative shaker test pseudo-damage could be achieved.

This work presents a solely comparative assessment of the pseudo-damage in different battery loading scenarios. A fatigue analysis could have been done so that the actual damage would be calculated. This step would be advantageous for the determination of the expected battery durability as well as for targeting new critical areas. FemFat is a well-known software to carry this type of analyses. By inputing the finite element model of the battery, the stress distribution present in each eigenmode, a time-history of all the modal participation factors, and the material mechanical properties, a numerical fatigue analysis can be carried.

7. Acknowledgements

The author of this work would like to take this opportunity to thank AVL List GmbH for the support given throughout the project and for the provided software licenses.

References

[1] Johannesson, M. Speckert. *Guide to Load Analysis for Durability in Vehicle Engineering*. Wiley, 2014.

[2] A. Dörnhofer. *Betriebsfestigkeitsanalyse elektrifzierter Fahrzeuge*. Springer, 2018.

[3] J. M. Hooper, J. Marco . Defining a Representative Vibration Durability Test for Electric Vehicle (EV) Rechargeable Energy Storage Systems (RESS). *World Electric Vehicle Journal*, 2016.

[4] McKinsey Report. Electromobility's impact on powertrain machinery, may 2021. https://www.mckinsey.com/industries/automotive-and-assembly/our-insights/electromobilitys-impact-on-powertrain-machinery Accessed: 2021-10-27.

[5] A. Rissoan. Damage and equivalent load definition for mechanical durability of subframe. Master's thesis, ENSTA Bretagne, 2018.

[6] S. BenZvi. Physics 403 - Spectral Analysis. https://www.pas.rochester.edu/~sybenzvi/courses/phy403/2015s/p403_21_spectral_analysis.pdf.